The MinC component of the division site selection system in *Escherichia coli* interacts with FtsZ to prevent polymerization

Zonglin Hu, Amit Mukherjee, Sebastien Pichoff, and Joe Lutkenhaus*

Department of Microbiology, Molecular Genetics and Immunology, University of Kansas Medical Center, Kansas City, KS 66160

Edited by Richard M. Losick, Harvard University, Cambridge, MA, and approved October 26, 1999 (received for review September 7, 1999)

Positioning of the Z ring at the midcell site in *Escherichia coli* is assured by the *min* system, which masks polar sites through topological regulation of MinC, an inhibitor of division. To study how MinC inhibits division, we have generated a MalE-MinC fusion that retains full biological activity. We find that MalE-MinC interacts with FtsZ and prevents polymerization without inhibiting FtsZ's GTPase activity. MalE-MinC19 has reduced ability to inhibit division, reduced affinity for FtsZ, and reduced ability to inhibit FtsZ polymerization. These results, along with MinC localization, suggest that MinC rapidly oscillates between the poles of the cell to destabilize FtsZ filaments that have formed before they mature into polar Z rings.

cell division | Z ring

Spatial regulation of cytokinesis is essential for the faithful distribution of the replicated chromosomes to daughter cells. This regulation positions a cytoskeletal element, which in bacteria is the Z ring, that defines the division plane (1, 2). The behavior of the Z ring has been documented by immunoelectron and fluorescence microscopy (2–4). The Z ring assembles at the future division site before cytokinesis and is at the leading edge of the invaginating septum throughout cytokinesis. The Z ring functions in part as a scaffold to assemble the machinery necessary for cytokinesis (1, 5, 6).

FtsZ is a structural and functional homologue of tubulin capable of undergoing dynamic assembly *in vitro* in the presence of GTP (7–10). FtsZ assembles into protofilaments that are structural homologues of the protofilaments present in microtubules (7, 11, 12). Further assembly of these protofilaments into sheets and bundles has been observed with various multivalent cations (7, 8, 12, 13) and ZipA (14). *In vivo*, the Z ring is likely to consist of 10–20 protofilaments of FtsZ wrapped around the cell. One model suggests that Z ring formation occurs in response to the activation of a nucleation site at midcell leading to bi-directional growth of the structure to eventually form the ring (15, 16).

The positioning of the Z ring at midcell is disturbed in *min* mutants (17). In such mutants, the Z ring can form at midcell or near the pole of the cell leading to formation of a minicell that lacks a chromosome (18). This phenotype suggests that the poles of cells contain nucleation sites for FtsZ assembly that are normally masked by the *min* system (19). Interestingly, overproduction of FtsZ also leads to minicell formation, suggesting competition between FtsZ and the *min* system for these polar sites (20).

In *Escherichia coli*, the *min* system encodes three proteins: MinC, MinD, and MinE (21). Genetic and expression studies indicate that MinC and MinD cooperate to form an inhibitor of cell division that lacks topological specificity. MinC alone, however, can inhibit division if the level is increased 25- to 50-fold above the physiological concentration (22). This suggests that MinC contacts the division machinery and that MinD activates MinC (22). Interaction between MinC and MinD has been observed in the yeast two-hybrid system, suggesting that the activation may involve direct association between these proteins (23). Recently, it has been shown that MinD is required to recruit MinC to the membrane (24–26).

The inhibitory activity of MinCD is topologically regulated by MinE in *E. coli* (21) and DivIVA in *Bacillus subtilis* (27, 28). These proteins protect the midcell site from the MinCD inhibitor but do this in different ways. MinE forms a ring near the cell center independent of FtsZ that induces MinC and MinD to rapidly oscillate between the halves of the cell without occupying midcell (25, 26, 29). In contrast, DivIVA is recruited to the nascent division site in an FtsZ-dependent manner (30). It then recruits MinC and MinD and restricts them to the cell poles after division (24, 28).

Although MinCD is a known inhibitor of division, the mechanism is unknown (18, 31). Genetic evidence suggests interaction with FtsZ because overexpression of FtsZ suppresses the inhibition by MinC (and MinCD), and certain alleles of *ftsZ* show increased resistance to inhibition by MinCD (31, 32). It is possible that MinCD blocks Z ring formation by masking nucleation sites or decreasing the stability of FtsZ polymers. To assess how MinC functions, we have purified a functional MalE-MinC fusion and have assessed its ability to interact with FtsZ.

Materials and Methods

Strains and Plasmids. The *E. coli* K12 strain JS964 (MC1061 *malP*::*lacI*^{q} Δ*min*::*kan*) was used in this study (33). The plasmid pJC90 was constructed by cloning *malE* into the polylinker of the expression plasmid pBAD18 downstream of the P_{BAD} promoter (34). The *malE* fragment flanked by *Nhe*I and *Hin*dIII sites was obtained by PCR using pMalc-2 (New England Biolabs) as a template. The primers for the PCR step were 5′-A*GCTAGC*AGGTGTTTTCACGAGCA-3′ (*Nhe*I site italicized) and 5′-CTTATCTCATCCGCCAA-3′ (complementary to a region downstream of the *Hin*dIII site at the 3′end of *malE*). Various fusions to *malE* were constructed by inserting PCR fragments at the 3′end of *malE* in pJC90. pZH101 (*malE-minC*) was constructed by inserting a PCR fragment digested with *Eco*RI and *Sal*I. The primers containing these restriction sites were 5′-TAGCAT*GAATTC*AGCAACACGCCAATCGAGCTTAAA-3′ and 5′-TAGCAT*GTCGAC*TCAATTTAACGGTTGAACGGTC-3′. The template was pJPB210 (*minCDE*). pZH102 (*malE-minC19*) was constructed as pZH101 except that pCL45 (*minC19*) was used as a template (35). pZH103, containing *minD*, was obtained by cloning the *Pst*I fragment from pJB210 into the *Pst*I site of pGB2 (36). The *minC* gene in pJPB210 (33) was inactivated by filling in the *Nsi*I site located within the *minC* gene. The resultant plasmid pZH104 expressed *minD* and *minE*. pBS58 contains *ftsQ*, *ftsA*, and *ftsZ* cloned in pGB2 (37).

This paper was submitted directly (Track II) to the PNAS office.

*To whom reprint requests should be addressed. E-mail: jlutkenh@kumc.edu.

The publication costs of this article were defrayed in part by page charge payment. This article must therefore be hereby marked "*advertisement*" in accordance with 18 U.S.C. §1734 solely to indicate this fact.

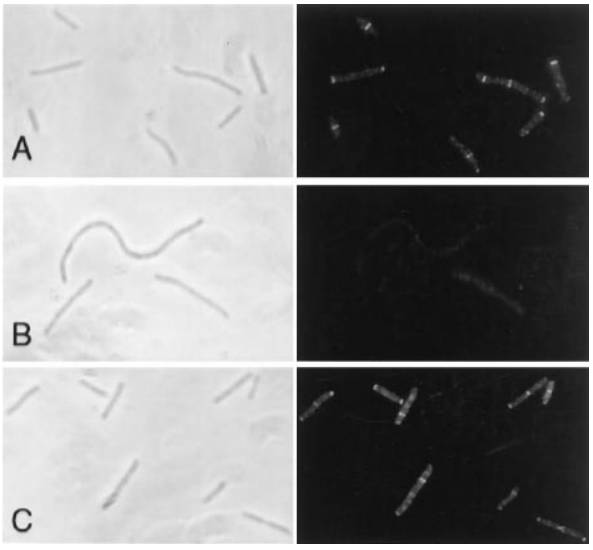

Fig. 1. Effect of MalE-MinC fusions on cell division. (*A* and *B*) The MalE-MinC fusion blocks cell division and Z ring formation. A culture of JS964 (Δ*min*) pZH101 (P_{BAD}::*malE-minC*) was processed for immunofluorescence microscopy before (*A*) and 1 hr after (*B*) addition of 0.01% arabinose. The cells were immunostained with antibodies to FtsZ, and a secondary antibody was conjugated to the fluorophore Cy3. The panels to the left are phase contrast micrographs, and those to the right are fluorescence micrographs. (*C*) A MalE-MinC19 fusion is attenuated for inhibition of cell division. JS964 (Δ*min*) pZH102 (P_{BAD}::*malE-minC19*) was induced with 0.01% arabinose for 1 hr, and a sample was taken and immunostained for FtsZ.

Protein Purification. FtsZ was purified as described (9). MalE, MalE-MinC, and MalE-MinC19 were purified from cultures of JS964 containing pJC90, pZH101, or pZH102, respectively. Overnight cultures were diluted 1:100 in LB medium containing 100 μg/ml ampicillin. When the OD_{600} reached 0.3, arabinose was added to 0.1% and, induction continued for 3 hr. Cells were harvested and lysed with a French press. Cell debris and membranes were removed by centrifugation at 12,000 rpm for 10 min and 38,000 rpm for 90 min (Beckman Ti50.2 rotor), respectively. The MalE fusions were purified from the high speed supernatant by amylose column chromatography as described by New England Biolabs except that 25 mM Tris·HCl (pH 7.4) was used instead of phosphate buffer. The fusion proteins were further purified by DEAE column chromatography.

Polymerization of FtsZ and Determination of GTPase Activity. FtsZ at the concentration indicated was incubated in polymerization buffer (50 mM Mes·NaOH, pH 6.5/10 mM $MgCl_2$/and 50 mM KCl). Any additions, such as the MalE fusions, were made at room temperature, with GTP added last to give a volume of 100 μl. Polymerization was monitored by electron microscopy or sedimentation as described (9). For sedimentation assays, the amount of FtsZ in the pellet was determined by solubilizing the pellet in 100 μl of SDS sample buffer and running 20 μl on SDS/PAGE. After staining with Coomassie brilliant blue, the bands were quantitated with digital imaging equipment from Alpha Innotech (San Leandro, CA). The GTPase activity of FtsZ was measured as described (9).

Yeast Two-Hybrid Assay. pJC41 (AD-MinD), pJC41-2 (BD-MinD), pJC22 (BD-MinC), and pJC22-1 (AD-MinC) and the parental vectors pGAD424 and pGBT9 were described previously (23). Additional plasmid constructs carried the *minC19* mutation and included pJC22-2 (BD-MinC19) and pJC22-3 (AD-MinC19). They were constructed by cloning restriction fragments obtained by PCR using pCL45 as a template. The primers used were the same as previously used in cloning wild-type *minC* (23). The plasmids were transformed into the SFY526 in various combinations and were analyzed for β-galactosidase production by the colony lift assay as described in the CLONTECH manual. The intensity of color development was compared with knowns.

Phenotypic Analysis of the MalE Fusions. The effect of MalE fusions on cell morphology was determined on plates or in liquid medium. JS964 containing pJC90, pZH101, or pZH102 was grown in LB containing ampicillin and was induced with 0.01% for 1 hr, and samples were taken for immunofluorescence microscopy (3). To test for the response of *minC* or *minC19* to *minD* or *minDE*, JS964 containing pZH101 or pZH102 was transformed with compatible plasmids containing *minD* (pZH103), *minDE* (pZH104), or the vector (pGB2). Transformants were selected on LB agar plates containing ampicillin and spectinomycin and were streaked on these plates containing the indicated concentrations of arabinose. Cell morphology was determined by phase contrast microscopy.

Biosenor Assay of Interaction Between FtsZ and MinC. Protein–protein interactions were examined at 25°C by using a biosensor-based analytical system (38). We used an IAsys Plus instrument and biotin cuvettes from Affinity Sensors (Cambridge, U.K.). FtsZ was biotinylated by using Sulfo-NHS-LC-biotin following the protocol provided by the manufacturer (Pierce, catalog no. 21335). The biotinylated FtsZ was immobilized via binding to streptavidin that had been bound to a biotin cuvette following the protocol provided by Affinity Sensors. The cuvette was washed with PBS, and then streptavidin was added to a final concentration of 10 μg/ml in a final volume of 60 μl of PBS. After 10 min the unbound streptavidin was removed with a PBS wash, and biotinylated FtsZ was added to a final concentration of 160 μg/ml for 10 min. The cuvette was washed with PBS and equilibrated with Pol buffer. In a typical experiment, the cuvette contained 1,000 arc seconds of streptavidin and 500 arc seconds of FtsZ. The MalE-MinC and MalE-MinC19 were added at different concentrations in a volume of 60 μl of Pol buffer, and the increase in arc seconds was measured versus time. The bound MinC protein was removed by incubation for 3 min in 4 M urea. Repeated washes with 4 M urea did not affect the binding capacity of FtsZ for MalE-MinC.

Results

A MalE-MinC Fusion Has Biological Activity: It Inhibits Division and Responds to MinD. Our strategy to investigate the mechanism of MinCD inhibition of cell division was to focus on MinC because overproduction studies suggest that MinC is the component of this bipartite inhibitor that contacts the division machinery (22).

Table 1. Phenotype of JS964 (Δ*min*) expressing various MalE-MinC fusions in the presence and absence of MinD*

	MalE-MinC		MalE-MinC19	
Arabinose, %	−MinD†	+MinD	−MinD	+MinD
None, glucose	Min	Fil	Min	Min
None	Min	Fil	Min	Min
0.0001	Min	Fil	Min	Min
0.001	Het	Fil	Min	Fil
0.01	Fil	Fil	Het	Fil

*Phenotypes: Min indicates typical minicell phenotype; Fil indicates that cells were filamentous; Het indicates that the cell population was a mixture of filaments and smaller cells.

†Strain JS964 containing pZH101 (*malE-minC*) or pZH102 (*malE-minC19*) was transformed with pGB2 (vector) or pZH103 (*minD*).

Table 2. Min protein interactions observed by the yeast two-hybrid system

DNA binding domain	Activaiton domain	Interaction*
MinC	–	–
MinD	–	–
MinC	MinD	++++
MinD	MinC	++
MinC19	–	–
MinC19	MinD	++++
MinD	MinC19	++

*Represents the strength of interaction based on the color development by using X-Gal (5-bromo-4-chloro-3-indolyl-β-D-galactoside). ++++, strong interaction and was previously measured at 160 units of β-galactosidase activity (23); +++, intermediate strength; ++, moderate strength and was previously measured at 48 units of β-galactosidase activity (23); + weak activity; –, no interaction because no color development was observed after 24 hr.

A *malE-minC* fusion was constructed under arabinose promoter control on a multicopy plasmid pZH101 and was introduced into JS964 (Δ*min*) to determine whether it retained ability to inhibit division. In the absence of arabinose, this strain, JS964 (pZH101), had a typical *min* phenotype, and Z rings were present (Fig. 1*A*; Table 1). These rings were present at the poles and at internal division sites typical of a Δ*min* mutant (18, 39). Induction of MalE-MinC with 0.01% arabinose led to rapid inhibition of cell division as cell length was noticeably increased by 1 hr (Fig. 1*B*) and Z ring formation was completely blocked. By 30 min, division was inhibited and the level of MalE-MinC was 50,000 molecules per cell (data not shown). This inhibition was suppressed by introduction of pBS58, a low copy plasmid that increases FtsZ 4- to 5-fold (data not shown).

The ability of the MalE-MinC fusion to cooperate with MinD to inhibit division was determined by introducing a compatible plasmid expressing *minD* (pZH103) into JS964 (Δ*min*) containing pZH101 (*malE-minC*). All transformants obtained were extremely filamentous, even those obtained in the presence of glucose (Table 1). In contrast, transformants of JS964 (Δ*min*) lacking the *minD* plasmid had a classical *min* phenotype on glucose and only displayed extensive filamentation when the arabinose concentration was 0.01% or greater (Table 1). This result indicated that MalE-MinC retains the ability to be activated by MinD to produce a more potent inhibitor of cell division. Finally, we introduced a compatible plasmid expressing *minDE* (pZH104) into JS964 (Δ*min*) containing pZH101. Introduction of this plasmid restored the wild-type division phenotype, indicating that MalE-MinC, like the GFP-MinC fusion studied previously (25), is fully functional (data not shown). Because the fusion retained these biological activities, JS964 (Δ*min*) containing pZH101 (*malE-minC*) was induced with 0.1% arabinose and the fusion protein was purified by affinity chromatography.

The *minC19* Mutation Affects the Interaction of MinC with the Division Machinery but Not with MinD. Many mutations have been isolated in *minC* that reduce its ability to inhibit cell division. Most of these mutations were isolated as refractory to activation by MinD and/or DicB (40). Although most of these mutations produce unstable proteins (41) the MinC19 mutant is stable and therefore appears resistant to activation by MinD and DicB. Although MinC19 might not interact with these activators, another possibility is that it does not interact with the division apparatus. One test of these two possibilities is to express MalE-MinC19 in the absence of MinD. Inability to inhibit division in the absence of MinD would suggest that MinC19 does not interact with the division apparatus.

A *malE-minC19* fusion was constructed under arabinose promoter control (pZH102) and was transformed into JS964 (Δ*min*). One hour after induction of an exponential culture with 0.01% arabinose, cell division was largely unaffected and Z rings were present (Fig. 1*C*). Thus, this fusion did not inhibit division or block Z ring formation as efficiently as MalE-MinC. Quantitative immunoblotting demonstrated that MalE-MinC19 was stable and induced to the same level as MalE-MinC (data not shown). On plates containing 0.01% arabinose, cell division was only slightly affected (Table 1). Importantly, these results demonstrate that the *minC19* mutation alters MinC such that it has a reduced interaction with the division apparatus.

Interestingly, introduction of a compatible plasmid expressing *minD* (pZH103) into JS964 (Δ*min*) containing pZH102 could still bring about filamentation, but only at high arabinose concentrations (Table 1). This is in contrast to the same strain expressing the wild-type MalE-MinC fusion, where filamentation was observed even in the absence of arabinose. Together,

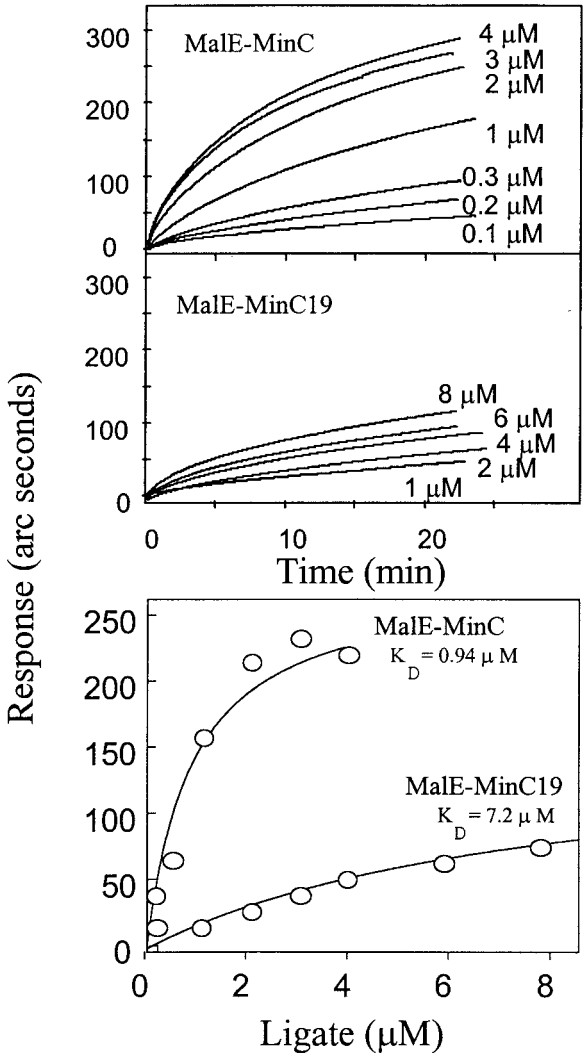

Fig. 2. Monitoring interactions between FtsZ and MalE-MinC fusions by using an optical biosensor. Biotinylated FtsZ was immobilized in a biotin cuvette as described in *Materials and Methods*. MalE-MinC or MalE-MinC19 was added at the concentrations indicated in a final volume of 60 μl, and the response in arc seconds was measured versus time (*Upper*). The data obtained from these experiments were analyzed with IASYS FASTFIT software by using single phase association to obtain the equilibrium binding plots and K_d values (*Lower*).

BIOCHEMISTRY

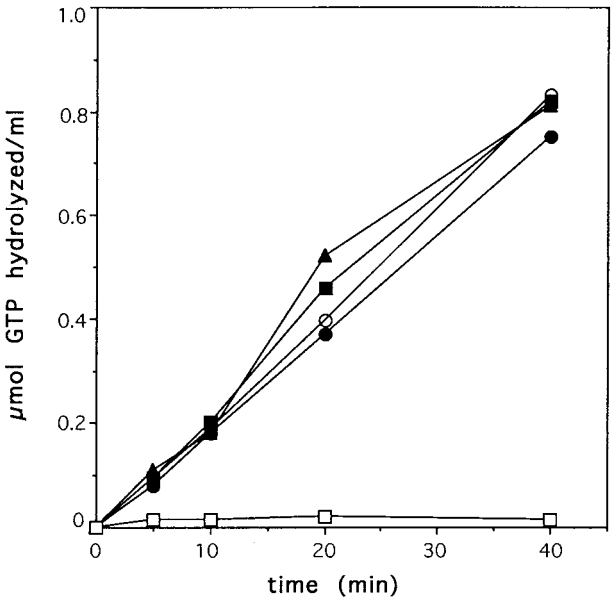

Fig. 3. MalE-MinC does not inhibit FtsZ's GTPase activity. The GTPase activity of FtsZ (5 μM) was measured in polymerization buffer containing increasing amounts of MalE-MinC. The reaction was initiated with the addition of GTP and was incubated at 30°C. At various times, samples were removed, and the amount of P_i hydrolyzed was determined. Shown is FtsZ alone (open circles) and FtsZ with the addition of MalE-MinC at 0.75 μM (filled circles), 3 μM (filled squares), and 12 μM (filled triangles). As a control, the GTPase activity of MalE-MinC (12 μM) was determined in the absence of FtsZ (open squares).

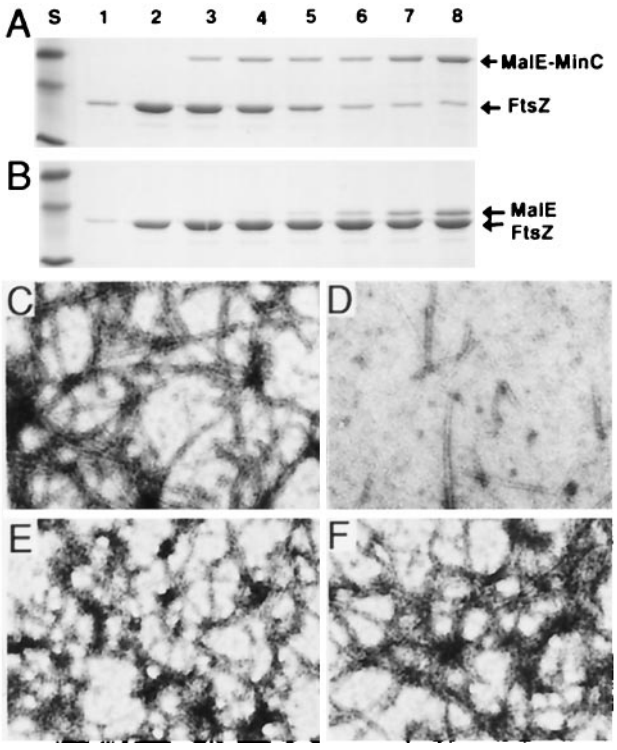

Fig. 4. The effect of MalE-MinC on FtsZ polymerization. (*A* and *B*) Polymerization reactions (100 μl) were carried out with FtsZ (5 μM) in polymerization buffer and increasing concentrations of MalE-MinC (*A*) or MalE (*B*). Polymerization was initiated with the addition of 1 mM GTP, samples were centrifuged, and the pellets were analyzed by SDS/PAGE. *A* shows the effect of MalE-MinC: lane 1, GDP added; lane 2, GTP added served as controls. The concentrations of MalE-MinC were, by lanes: 3, 50 μg/ml (0.75 μM); 4, 100 μg/ml (1.5 μM); 5, 200 μg/ml (3 μM); 6, 400 μg/ml (6 μM); 7, 800 μg/ml (12 μM); 8, 1200 μg/ml (18 μM); (*B*) As *A* except that MalE was added instead of MalE-MinC. The concentrations (in μg/ml) were the same as in *A*. (*C–E*) Samples were also taken 10 min after GTP addition and were examined by electron microscopy. *C* contained FtsZ alone (5 μM); *D* contained FtsZ (5 μM) with 3 μM (200 μg/ml) of MalE-MinC; *E* contained FtsZ (5 μM) and MalE at 200 μg/ml; and *F* contained FtsZ (5 μM) and MalE-MinC19 at 200 μg/ml).

these results suggest that MalE-MinC19 is attenuated in its ability to interact with the division apparatus, but, at high levels, and especially in the presence of MinD, it is still able to inhibit division. This latter result suggests that MinC19 still interacts with MinD. This possibility was examined by using the yeast two-hybrid system. We previously found that MinC and MinD interact strongly in this test system (23). Substituting MinC19 for MinC did not affect the interaction with MinD (Table 2). JS964 (Δ*min*) containing pZH102 (*malE-minC19*) was induced with 0.1% arabinose, and the fusion protein was purified by affinity chromatography.

Interaction of MinC and MinC19 with FtsZ Tested with a Biosensor. To look for an interaction between MinC and FtsZ, we exploited biosensor technology. In these experiments, FtsZ was biotinylated and immobilized through binding to streptavidin, which was bound to a biotin cuvette. The immobilization was done at 4 μM FtsZ (160 μg/ml). MalE-MinC or MalE-MinC19 was then introduced into the cuvette at various concentrations, and the response was measured (Fig. 2 *Upper*). At each concentration of the fusions, the magnitude of the response was always greater with the MalE-MinC fusion than with the MalE-MinC19 fusion. The calculated K_d from this data is 0.9 μM for MalE-MinC and 7.3 μM for MalE-MinC19 (Fig. 2 *Lower*). These experiments demonstrate that MinC binds to FtsZ and that the *minC19* mutation reduces the affinity.

MinC Inhibits Polymerization of FtsZ but Not FtsZ's GTPase. FtsZ undergoes dynamic assembly in the presence of GTP (9, 42). As a first step in assessing the effect of MinC on the activity of FtsZ, we examined the effect of MalE-MinC on FtsZ's GTPase activity. As shown in Fig. 3, MalE-MinC did not inhibit FtsZ's GTPase activity. Even at a molar excess, MalE-MinC (12 μM MalE-MinC to 5 μM FtsZ) did not have a significant effect on FtsZ's GTPase activity. Because the GTPase activity of FtsZ displays a dramatic dependence on the FtsZ concentration, it suggests that an interaction between FtsZ molecules is required (43, 44). Our results argue that MalE-MinC does not inhibit this association.

To assess the effect of MalE-MinC on polymerization, we used a sedimentation assay. Increasing amounts of MalE-MinC were incubated with FtsZ (5.0 μM), the reactions were centrifuged, and the pellet was analyzed by SDS/PAGE. The results (Fig. 4*A*) show that MalE-MinC, in a concentration-dependent manner, reduced the amount of FtsZ recovered in the pellet. At approximately a 1:1 ratio of MalE-MinC to FtsZ, the amount of FtsZ in the pellet was reduced to the control level (Fig. 4*A*, compare lanes 6 and 1). This suggests that FtsZ polymerization was completely inhibited. As a control, we performed the polymerization assay using the same concentration of MalE and found no inhibition of polymerization (Fig. 4*B*).

In the sedimentation assay, the samples were centrifuged and aspirated, and the pellets were solubilized and analyzed by SDS/PAGE. Although some MalE is present in the pellets, it was no more than observed in control reactions lacking FtsZ (data not shown). With MalE-MinC, however, there were significant levels in the pellet, especially at low concentrations of MalE-MinC (Fig. 4*A*). Quantitation of the reaction containing 50 μg/ml of MalE-MinC revealed that 36% of the MalE-MinC

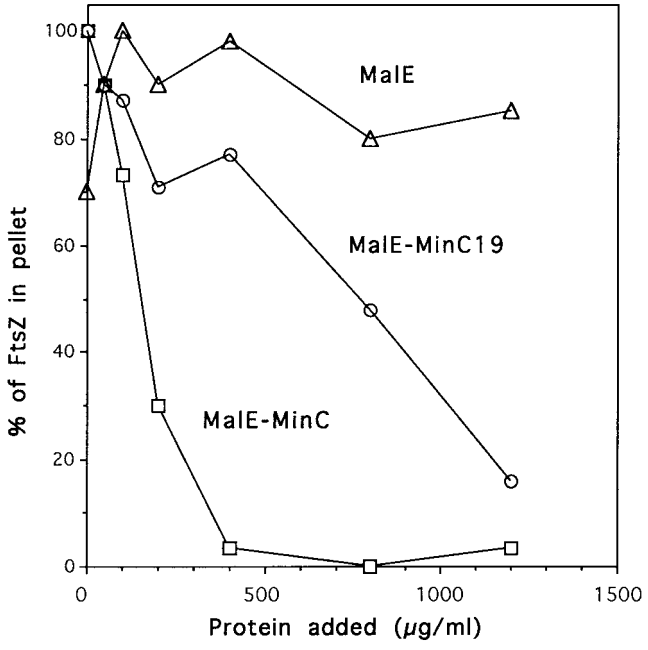

Fig. 5. MalE-MinC19 has reduced inhibitory activity in the FtsZ assembly assay. FtsZ was incubated with increasing amounts of MalE-MinC19 in polymerization buffer. Assembly was initiated with 1 mM GTP, and samples were centrifuged and were analyzed by SDS/PAGE. The amount of FtsZ in the pellet was quantitated and plotted along with the results obtained with MalE and MalE-MinC additions (data from Fig. 4). The amount of FtsZ in the pellet in the absence of MalE or the fusions was set at 100%. This represents ≈50% of the FtsZ in the reaction (9, 42).

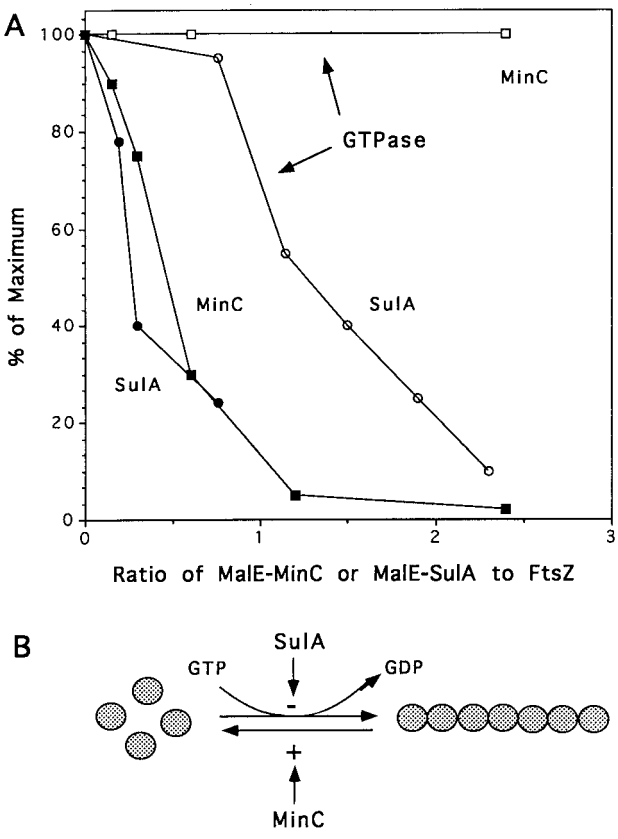

Fig. 6. Comparison of the effects of MinC and SulA on FtsZ. (*A*) The data obtained previously for SulA's effect on FtsZ (45) are plotted along with the results of MinC obtained in this study. The GTPase activity and amount of polymer obtained in the absence of inhibitor was set at 100%. The fractional values obtained in the presence of the inhibitors are plotted versus the molar ratio of inhibitor to FtsZ. For the purposes of comparison we have assumed the inhibitor is a monomer. The open symbols are GTPase activity, and the filled symbols are for polymerization. (*B*) This diagram contrasts the different steps affected by the two inhibitors. SulA blocks the GTPase activity and polymerization. In contrast, MinC prevents net assembly of FtsZ without inhibiting the GTPase activity, arguing that it promotes disassembly.

was in the pellet compared with 12% in the absence of FtsZ. This result indicates that MalE-MinC binds to FtsZ filaments.

To confirm the results obtained with the sedimentation assay, the effect of MalE-MinC on FtsZ polymerization was also examined by electron microscopy. Abundant FtsZ polymers were observed in the control reaction shown in Fig. 4*C*. The addition of increasing concentrations of MalE-MinC led to a progressive decrease in the length and number of polymers. For example, the reaction containing MalE-MinC at 200 μg/ml (3.0 μM) produced shorter and fewer filaments (Fig. 4*D*), consistent with the sedimentation results at this concentration (Fig. 4*A*, lane 5). In contrast, the addition of MalE at 200 μg/ml did not have a detectable effect on the quantity of polymers (Fig. 4*E*), again consistent with the sedimentation results (Fig. 4*B*, lane 5).

MinC19 Is a Less Effective Inhibitor of FtsZ. To further examine the effect of the *minC19* mutation on the interaction of MinC with FtsZ, we examined the effect of MalE-MinC19 on the polymerization of FtsZ. Electron microscopy of a polymerization reaction containing 200 μg/ml MalE-MinC19 revealed no effect on FtsZ polymerization (Fig. 4*F*). This result was consistent with the sedimentation assay that indicated that MalE-MinC19 did not inhibit FtsZ polymerization nearly as efficiently as the wild-type fusion (Fig. 5). MalE-MinC19 did, however, inhibit polymerization more than MalE, suggesting it has residual activity. This is consistent with MalE-MinC19 having residual inhibitory activity *in vivo* when expressed at high levels. Thus, MinC19 has decreased ability to interact with FtsZ and is attenuated for the inhibitory activity on FtsZ polymerization.

Comparison of the Effects of MinC and SulA on FtsZ. SulA, an inducible component of the SOS system, has previously been shown to block FtsZ polymerization (45, 46). The effects of MalE-MinC and SulA on polymerization and GTPase activity are compared in Fig. 6*A*. This plot (data for SulA is from ref. 45) shows that MinC is as effective as SulA in blocking polymer formation (assayed by sedimentation). However, SulA blocks FtsZ's GTPase activity whereas MalE-MinC has no effect. Our results suggest that MalE-MinC acts at a step in polymerization, after the interaction of FtsZ subunits that results in GTPase activity, presumably destabilizing the filaments. This difference in mode of action of MinC and SulA on inhibiting FtsZ polymerization is diagrammed in Fig. 6*B*.

Discussion

The *min* system prevents minicell formation through topological regulation of the MinCD inhibitor. In this study, we focused on the MinC component of this bipartite inhibitor because it was thought to contact the division machinery. The major finding in this study is that MinC interacts directly with FtsZ and prevents polymerization. These results, along with the localization results of MinC (25, 26), suggest a model for how minicell formation is prevented. In this model, MinC oscillates between the cell poles where it destabilizes nascent FtsZ polymers before they mature into a functional Z ring.

To study the activity of MinC, we used a MalE-MinC fusion that was fully functional; it inhibited division and was activated by MinD.

BIOCHEMISTRY

Using both sedimentation and electron microscopy, we found that MalE-MinC decreased the length and amount of FtsZ polymers in a concentration-dependent manner. The near stoichiometry of the inhibition *in vitro* is in line with level of MalE-MinC reached *in vivo*, which is in excess of the FtsZ level [20,000 molecules per cell (2)]. On a molar basis, the inhibitory activity of MalE-MinC is comparable to the activity of MalE-SulA (Fig. 6*A*). The action of these two inhibitors must be quite different, however, because MalE-SulA blocks the GTPase activity of FtsZ whereas MalE-MinC does not. We interpret this difference as MalE-SulA blocking productive interaction between FtsZ subunits that triggers GTP hydrolysis whereas MalE-MinC acts at a step after interaction of FtsZ subunits. Because MinC binds to FtsZ polymers, it may increase the off rate of FtsZ subunits or cause severing of the filaments. This mode of action would be similar to the ADF/cofilin family of proteins that bind to actin filaments and cause disassembly (47, 48). However, the precise mechanism by which MinC functions to limit polymer mass is unknown and is the subject of future study.

Our studies of MalE-MinC indicate that it is a fairly effective inhibitor of FtsZ polymerization, even in the absence of MinD. *In vivo*, the activity of MinC is augmented ≈25- to 50-fold by the presence of MinD (22). How does MinD augment MinC's activity? One possibility is that association between MinD and MinC could affect the affinity of MinC for FtsZ or the MinCD complex could be more active in dissociating FtsZ polymers. However, in recent experiments, we observed no enhancement of MinC's inhibitory activity by MinD, suggesting another mechanism (data not shown). As shown earlier, MinD recruits MinC to the membrane (24–26), and restricting a cytoplasmic protein to the surface of the membrane would result in a 20- to 50-fold increase in the concentration at the membrane. This partitioning of MinC to the membrane by MinD could fully account for the magnitude of this activation, as we have suggested earlier (25).

In these studies, we have also analyzed MinC19, which has Asp substituted for Gly at position 10 in the mutant protein. Our initial characterization of MinC19 took advantage of MinC's ability to inhibit division in the absence of MinD. Revealingly, MinC19 was attenuated in its ability to inhibit division, suggesting that it was deficient in contacting the division machinery. High levels of MalE-MinC19, however, especially in the presence of MinD, resulted in division inhibition. This result argued that MinC19 had residual inhibitory activity and suggested that the interaction between MinC and MinD was not altered by the *minC19* mutation. Consistent with this, MinC19 interacted with MinD in the yeast two-hybrid system. Thus, MinD and MinC19 are able to cooperate *in vivo*, but the decreased ability of MinC19 to inhibit division makes the complex a less efficient inhibitor.

The primary effect of the *minC19* mutation is to decrease the interaction of MinC with the division apparatus. We determined that the K_d for the interaction between MinC and FtsZ was 0.94 μM. Furthermore, we determined that the K_d for FtsZ was increased ≈8-fold by the *minC19* mutation. The magnitude of this decrease in affinity correlates with a 6-fold reduction in MinC19's ability to inhibit FtsZ polymerization (Fig. 5). Importantly, MalE-MinC19's reduced ability to interact with FtsZ correlates with its reduced ability to inhibit division. These results argue strongly that MinC contacts the division machinery through FtsZ.

The studies of the *min* system in *E. coli* and *B. subtilis* reveal two alternative mechanisms for localizing MinC. In *E. coli*, MinC and MinD are found at the poles, but, rather than being retained at the pole, they flip-flop between the two poles (25, 26, 29). This oscillation depends on MinE, which forms a ring at the cell center independent of FtsZ (49). In *B. subtilis*, MinC is retained at the old pole by interaction with MinD, which in turn is anchored by DivIVA (24, 27, 28). These proteins are recruited to the septum by the Z ring after progression past a MinCD-sensitive step. A major difference between the localization of the Min proteins in these two systems is that the *B. subtilis* system is FtsZ-dependent whereas the *E. coli* system is FtsZ-independent. In both cases, though, the MinC inhibitor is placed on the membrane by interaction with MinD. Through this interaction, it is in position to destabilize FtsZ filaments that may form near the pole.

We gratefully acknowledge J. P. Bouche for providing pCL45. This work was supported by grant GM 29764 from the National institutes of Health.

1. Lutkenhaus, J. & Addinall, S. G. (1997) *Annu. Rev. Biochem.* **66,** 93–116.
2. Bi, E. & Lutkenhaus, J. (1991) *Nature (London)* **354,** 161–164.
3. Addinall, S. G., Bi, E. & Lutkenhaus, J. (1996) *J. Bacteriol.* **178,** 3877–3884.
4. Sun, Q. & Margolin, W. (1998) *J. Bacteriol.* **180,** 2050–2056.
5. Rothfield, L. I. & Justice, S. S. (1997) *Cell* **88,** 581–584.
6. Bramhill, D. (1997) *Annu. Rev. Cell Dev. Biol.* **13,** 395–424.
7. Mukherjee, A. & Lutkenhaus, J. (1994) *J. Bacteriol.* **176,** 2754–2758.
8. Erickson, H. P., Taylor, D. W., Taylor, K. A. & Bramhill, D. (1996) *Proc. Natl. Acad. Sci. USA* **93,** 519–523.
9. Mukherjee, A. & Lutkenhaus, J. (1998) *EMBO J.* **17,** 462–469.
10. Lowe, J. & Amos, L. (1998) *Nature (London)* **391,** 203–206.
11. Erickson, H. P. & Stoffler, D. (1996) *J. Cell Biol.* **135,** 5–8.
12. Lowe, J. & Amos, L. A. (1999) *EMBO J.* **18,** 2364–2371.
13. Yu, X.-C. & Margolin, W. (1997) *EMBO J.* **16,** 5455–5463.
14. RayChaudhuri, D. (1999) *EMBO J.* **18,** 2372–2383.
15. Lutkenhaus, J. (1993) *Mol. Microbiol.* **9,** 404–409.
16. Addinall, S. G. & Lutkenhaus, J. (1996) *Mol. Microbiol.* **22,** 231–238.
17. Adler, H. I., Fischer, W. D., Cohen, A. & Hardigree, A. A. (1967) *Proc. Natl. Acad. Sci. USA* **57,** 321–326.
18. Bi, E. & Lutkenhaus, J. (1993) *J. Bacteriol.* **175,** 1118–1125.
19. Teather, R. M., Collins, J. F. & Donachie, W. D. (1974) *J. Bacteriol.* **118,** 407–413.
20. Ward, J. E., Jr. & Lutkenhaus, J. (1985) *Cell* **42,** 941–949.
21. de Boer, P. A. J., Crossley, R. E. & Rothfield, L. I. (1989) *Cell* **56,** 641–649.
22. de Boer, P. A. J., Crossley, R. E. & Rothfield, L. I. (1992) *J. Bacteriol.* **174,** 63–70.
23. Huang, J., Cao, C. & Lutkenhaus, J. (1996) *J. Bacteriol.* **178,** 5080–5085.
24. Marston, A. L. & Errington, J. (1999) *Mol. Microbiol.* **33,** 84–96.
25. Hu, Z. & Lutkenhaus, J. (1999) *Mol. Microbiol.* **34,** 82–90.
26. Raskin, D. M. & de Boer, P. A. (1999) *J. Bacteriol.* **81,** 6419–6424.
27. Cha, J. H. & Stewart, G. C. (1997) *J. Bacteriol.* **179,** 1671–1683.
28. Marston, A. L., Thomaides, H. B., Edwards, D. H., Sharpe, M. E. & Errington, J. (1998) *Genes Dev.* **12,** 3419–3430.
29. Raskin, D. M. & de Boer, P. A. (1999) *Proc. Natl. Acad. Sci. USA* **96,** 4971–4976.
30. Edwards, D. H. & Errington, J. (1997) *Mol. Microbiol.* **24,** 905–916.
31. de Boer, P. A. J., Crossley, R. E. & Rothfield, L. I. (1990) *Proc. Natl. Acad. Sci. USA* **87,** 1129–1133.
32. Bi, E. & Lutkenhaus, J. (1990) *J. Bacteriol.* **172,** 5610–5616.
33. Pichoff, S., Vollrath, B., Touriol, C. & Bouche, J.-P. (1995) *Mol. Microbiol.* **18,** 321–329.
34. Guzman, L.-Z., Belin, D., Carson, M. J. & Beckwith, J. (1995) *J. Bacteriol.* **177,** 4121–4130.
35. Labie, C., Bouche, F. & Bouche, J.-P. (1990) *J. Bacteriol.* **172,** 5852–5855.
36. Churchward, G., Belin, D. & Nagamine, Y. (1984) *Gene* **31,** 165–171.
37. Bi, E. & Lutkenhaus, J. (1990) *J. Bacteriol.* **172,** 2765–2768.
38. Yeung, D., Gill, A., Maule, C. H. & Davies, J. A. (1995) *Trends Anal. Chem.* **14,** 49–56.
39. Yu, X.-C. & Margolin, W. (1999) *Mol. Microbiol.* **32,** 315–326.
40. Tetart, F. & Bouche, J. P. (1992) *Mol. Microbiol.* **6,** 615–620.
41. Sen, M. & Rothfield, L. I. (1998) *J. Bacteriol.* **180,** 175–177.
42. Mukherjee, A. & Lutkenhaus, J. (1999) *J. Bacteriol.* **181,** 823–832.
43. Wang, X. & Lutkenhaus, J. (1993) *Mol. Microbiol.* **9,** 435–442.
44. Lu, C., Stricker, J. & Erickson, H. P. (1998) *Cell Motil. Cytoskeleton* **40,** 71–86.
45. Mukherjee, A., Cao, C. & Lutkenhaus, J. (1998) *Proc. Natl. Acad. Sci. USA* **95,** 2885–2890.
46. Trusca, D., Scott, S., Thompson, C. & Bramhill, D. (1999) *J. Bacteriol.* **180,** 3946–3953.
47. Carlier, M. F., Laurent, V., Santolini, J., Melki, R., Didry, D., Xia, G. X., Hong, Y., Chua, N. H. & Pantaloni, D. (1997) *J. Cell Biol.* **136,** 1307–1322.
48. Blanchoin, L. & Pollard, T. (1998) *J. Biol. Chem.* **273,** 25106–25111.
49. Raskin, D. M. & de Boer, P. A. J. (1997) *Cell* **91,** 685–694.